Increased Ion Temperature and Neutron Yield Observed in Magnetized Indirectly Driven math xmlns="http://www.w3.org/1998/Math/MathML" display="inline">mrow>msub>mrow>mi mathvariant="normal">D/mi>/mrow>mrow>mn>2/mn>/mrow>/msub>/mrow>/math>-Filled Capsule Implosions on the National Ignition Facility

J. D. Moody et al.

Phys. Rev. Lett. **129**, 195002 — Published 4 November 2022

DOI: 10.1103/PhysRevLett.129.195002

Increased ion temperature and neutron yield observed in magnetized indirectly driven D_2-filled capsule implosions on the National Ignition Facility

J. D. Moody,[1] B. B. Pollock,[1] H. Sio,[1] D. J. Strozzi,[1] D. D.-M. Ho,[1] C. A. Walsh,[1] G. E. Kemp,[1] B. Lahmann,[1] S. O. Kucheyev,[1] B. Kozioziemski,[1] E. G. Carroll,[1] J. Kroll,[1] D. K. Yanagisawa,[1] J. Angus,[1] B. Bachmann,[1] S. D. Bhandarkar,[1] J. D. Bude,[1] L. Divol,[1] B. Ferguson,[1] J. Fry,[1] L. Hagler,[1] E. Hartouni,[1] M. C. Herrmann,[1] W. Hsing,[1] D. M. Holunga,[1] N. Izumi,[1] J. Javedani,[1] A. Johnson,[1] S. Khan,[1] D. Kalantar,[1] T. Kohut,[1] B. G. Logan,[1] N. Masters,[1] A. Nikroo,[1] N. Orsi,[1] K. Piston,[1] C. Provencher,[1] A. Rowe,[1] J. Sater,[1] K. Skulina,[1] W. A. Stygar,[1] V. Tang,[1] S. E. Winters,[1] G. Zimmerman,[1] P. Adrian,[2] J. P. Chittenden,[3] B. Appelbe,[3] A. Boxall,[3] A. Crilly,[3] S. O'Neill,[3] J. Davies,[4] J. Peebles,[5] and S. Fujioka[6]

[1] *Lawrence Livermore National Laboratory, Livermore, California 94550, USA*
[2] *Massachusetts Institute of Technology, Cambridge, MA 02139, USA*
[3] *Imperial College, London, UK*
[4] *University of Rochester, New York 14623, USA*
[5] *Laboratory for Laser Energetics, New York 14623, USA*
[6] *Institute for Laser Engineering, Japan*

(Dated: September 21, 2022)

Application of an external 26 Tesla axial magnetic field to a D_2 gas-filled capsule indirectly driven on the National Ignition Facility (NIF) is observed to increase the ion temperature 40% and the neutron yield a factor of 3.2 in a hot-spot with areal density and temperature approaching what is required for fusion ignition [1]. The improvements are determined from energy spectral measurements of the 2.45 MeV neutrons from the D(d,n)^{3}He reaction and the compressed central core B-field is estimated to be ~ 4.9 kT using the 14.1 MeV secondary neutrons from the D(T,n)^{4}He reactions. The experiments use a 30 kV pulsed-power system to deliver a $\sim 3\mu$s current pulse to a solenoidal coil wrapped around a novel high-electrical-resistivity $AuTa_4$ hohlraum. Radiation magneto-hydrodynamic simulations are consistent with the experiment.

PACS numbers: 52.57.-z, 52.25.Xz, 25.60.Pj

Since November 2020 a number of ICF experiments at the NIF have rapidly surpassed major milestones in plasma physics fusion research including a burning plasma [3, 4] and an igniting plasma [1] where alpha particle reheating from fusion reactions dominates all other forms of heating or power loss in the plasma. Following the first igniting plasma experiment in August 2021 several repeat and close variation experiments produced less than half of the original yield suffering degradations thought to be due mainly to target quality and laser delivery variations within what is currently achievable. A robust igniting plasma with reliable high yield on each shot given the available target and laser technology would have significant impact on frontier physics research of igniting plasmas as well as inertial fusion energy (IFE) schemes. Magnetized fusion fuel is one method of increasing implosion robustness and performance and a first test of this on NIF is described here.

The concept of combining inertial and magnetic confinement (magneto-inertial confinement) dates back at least to 1962 and the work of George Linhart [5]. Magnetized ICF involves pre-magnetizing the cryogenic deuterium-tritium (DT) fuel layer grown on the inside of the ablator prior to implosion with a laser, x-ray or pulsed power driver. The initial seed magnetic field becomes "frozen-in" to the fuel plasma and is amplified in simulations with perfect flux conservation by the factor C_R^2 [2, 5–17, 19–21] as the capsule implodes. C_R is the convergence ratio or the ratio of the initial inner capsule radius to the final fuel radius at full compression. Runaway self-heating nuclear fusion requires the power production from D-T generated alphas reheating the fuel to exceed the losses from thermal conduction and radiation. Magnetizing the fusion fuel reduces electron thermal conduction losses (main loss in NIF ICF implosions) orthogonal to the direction of the B-field if the Hall parameter, $\omega_{ce}\tau_{ei} \geq 1$ where ω_{ce} is the electron cyclotron frequency and τ_{ei} is the electron-ion collision time. The Braginskii formalism for magnetized plasma heat transport shows that for a large Hall parameter and a simple unidirectional B-field the average electron thermal conductivity, κ, decreases to 1/3 of the unmagnetized value [22]. The imploded magnetized core plasma temperature, which scales as $\kappa^{-2/7}$ [23], is estimated to increase by $\sim 40\%$ and the yield to increase by a factor of 1.8. For typical NIF implosion designs the Hall parameter, $\omega_{ce}\tau_{ei}$, is ~ 8 [24] (using B = 5 kT, $T_e = 4$ keV, and $n_e = 2.9 \times 10^{24}$/cc). In addition, 3.5 MeV alphas from the D-T fusion reactions stay longer in the core where they deposit more of their energy since their gyro-radius is smaller than the hot-spot. Self-generated Biermann battery fields in the hot-spot are seen in Gorgon simulations to reside mostly in a thin ($< 5\mu$m) layer at the colder hot-spot edge where they give an electron Hall parameter of ≤ 1 [25]. As a result their impact on the hot-spot temperature or yield in either unmagnetized or

magnetized implosions is negligible. The experimental results presented here test the effect of magnetization in a room-temperature indirect drive implosion and show a 40% temperature increase and a factor of 3.2 increase in yield. We expect these observed improvements to carry over in a quantitatively similar way to cryo-layered implosions and increase our confidence that magnetized DT ice-layered implosion designs will show a significant performance improvement and robustness.

The fusion rate per unit mass scales as $\sim \rho T_{th}^n$ where $n \sim 7/T_{th}^{0.2}$ [26] which means that a higher temperature hot-spot from magnetic insulation can boost marginally igniting designs to the runaway self-heating regime. Here T_{th} is the plasma thermal temperature (in keV) and ρ is the plasma density. The applied B-field may also mitigate radiative cooling due to mixing of high-Z capsule and fill-tube material into the fuel and hot-spot [27, 28] by reducing the growth of short scalelength hydrodynamic instabilities [29–31] as seen in 2D and 3D simulations [2, 20]. The seed field is most effective at boosting designs close to the ignition boundary to ignition but offers only a modest improvement for already igniting designs or ones significantly far from ignition [2]. Previous work on magnetizing ICF fuel [6–8, 11, 12, 14–18] using direct drive and pulsed power configurations verified the fundamentals of magnetized implosions and showed performance improvements in good agreement with simulations. Our results are the first to show yield and T_{ion} improvement in a magnetized indirect drive hot-spot with both ICF relevant ρR and scalesize larger than the Larmor radius of a 1.01 MeV triton (nearly identical to a 3.1 MeV D-T alpha particle). The $> 2\times$ higher fuel areal density, $\langle \rho R \rangle = \int \rho dr \sim 60$ mg/cm^2 and 40% higher ion temperature than previous experiments places the hot-spot in a regime of collisionality where thermal transport and ion energy slowing down are significantly closer to an igniting hot-spot.

The experiments are conducted on the 192 beam NIF laser which can direct up to 1.9 MJ of 351 nm laser light onto a target [32]. The beams are arranged in 2x2 arrays (quads) and enter the high-Z hohlraum through one of two laser entrance holes (LEH) in the top and bottom of the target, as shown in Fig. 1 (a). The lasers strike the inside hohlraum wall in an inner (near to the equatorial midplane) and outer (near to the LEHs) cone arrangement generating x-ray drive. The hohlraum is $\sim 20\mu$m thick of a novel high electrical resistivity, $\sim 200\mu\Omega$-cm, alloy of 20% atomic Au and 80% atomic Ta [33–36] (pure Au has resistivity $\sim 2\mu\Omega$-cm) with a 120 μm thick epoxy overcoat for mechanical stability. The B-field diffusion time through the hohlraum wall is measured with a B-dot probe to be about 20 ns and matches the theoretical estimate [37]. The hohlraum is magnetized by running current through 26-gauge Kapton-coated Cu wire wound on the hohlraum with 3 turns above and 3 below the midplane [see Fig. 1 (a)]. A 1.2 mm gap between the upper and lower coils allows for equatorial x-ray imaging of the implosion. A 4 μF capacitor charged to 30 kV achieves a peak coil current of 30 kA in about 3 μs; this gives a peak field of 26 T measured off-line with a B-dot probe placed at the capsule location. Peak current is timed to occur when the NIF lasers fire.

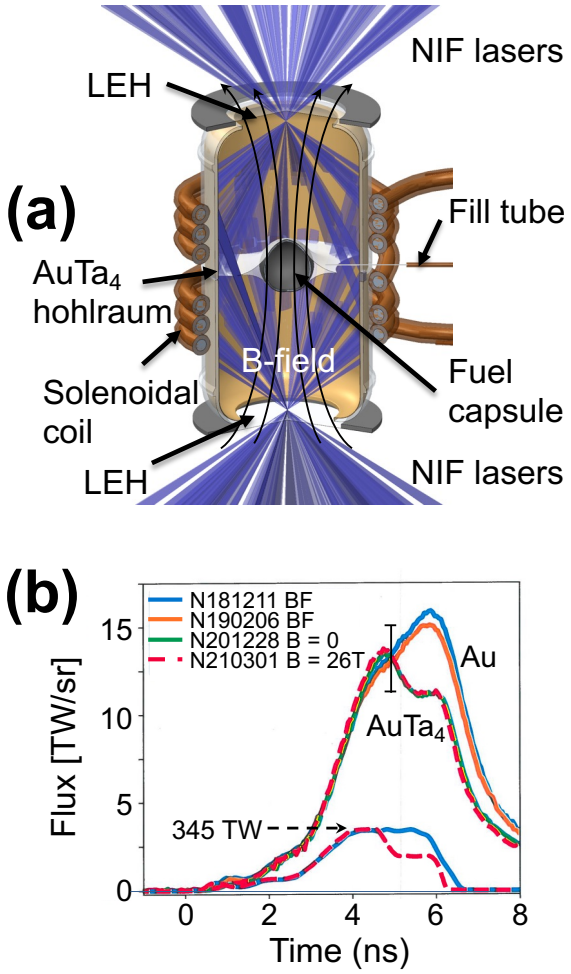

FIG. 1. (a) Sketch of the magnetized NIF hohlraum constructed from $AuTa_4$ with solenoidal coil to carry current. (b) X-ray drive measured through one of the LEHs and the incident laser powers for a magnetized and unmagnetized $AuTa_4$ hohlraum and two unmagnetized Au hohlraums. "BF" refers to "Big Foot," the name of the previous ignition design [38].

The implosion is a modification of a previous high-density carbon (HDC) ignition design [38]. The capsule inner radius is 844 μm, thickness is 64 microns with a 25 μm layer of 0.35% atomic W dopant starting 5 microns from the inner surface, it is filled with $\sim$ 3.9 mg/cc of pure D_2 through a 10 micron diameter glass fill-tube and is held in the center of the hohlraum with two 40-nm formvar tents. The hohlraum is filled with 0.24 mg/cc of C_5H_{12} gas at 293 K. The total laser energy cannot exceed 0.95 MJ due to pulser pre-fire backscatter risk. A failsafe protection system is being added to allow the maximum NIF energy for future experiments. Laser backscatter is measured to be below 2% for all shots discussed here.

Figure 1 (b) compares the measured x-ray drive vs time [39] of two unmagnetized Au hohlraums (N181211 and N190206) with an unmagnetized and magnetized $AuTa_4$ hohlraum. Also plotted is the total laser power for one unmagnetized Au hohlraum (the other is similar) and the magnetized $AuTa_4$ hohlraum which reach a peak power of 345 TW. Within the 17% measurement and analysis uncertainty the x-ray flux shows no measurable difference between Au and $AuTa_4$ and B = 0 and B = 26 T up to 4.5 ns when the laser pulses for Au and $AuTa_4$ diverge. The hot-spot ion temperature is inferred from the Doppler width [40] of the spectrum of emitted neutrons from the D(D,n)^{3}He reactions, centered at 2.45 MeV, using neutron time of fight (NTOF) detectors [41, 42]. Tritons at 1.01 MeV, generated from the D(D,p)T reactions, create secondary D-T neutrons with energy ranging from 11.9 to 17.2 MeV and represent about 1% of the total [43].

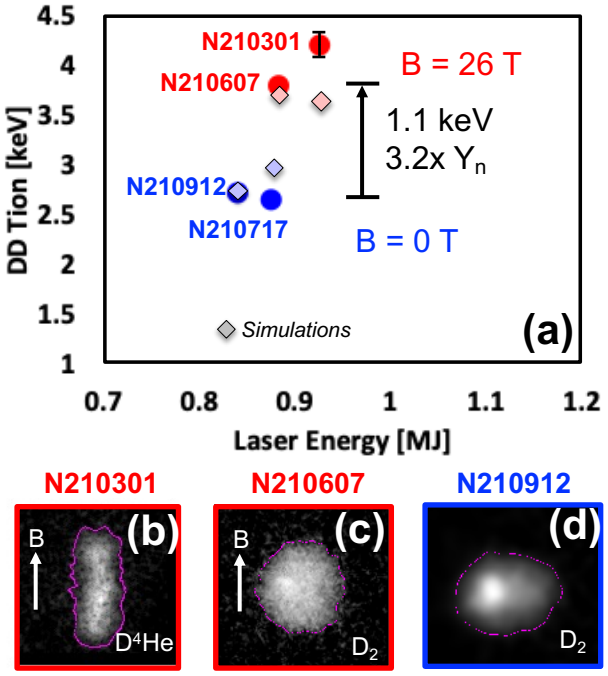

FIG. 2. (a) Plot shows that T_{ion} increases about 1.1 keV when adding a 26 T B-field to a D_2 gas capsule implosion. Also shown in the plot are the simulation results. (b) - (d) show the equatorial shapes of the implosions.

Figure 2 (a) shows T_{ion} vs laser energy for four experiments, two magnetized at 26 T and two unmagnetized. Table I lists the input parameters, key measurements and simulation results for six experiments including the four shown in Fig. 2 (a). Shots N201228 and N210620 had no capsule fill due to a blocked fill tube. Magnetized implosion N210607 shows a 1.1 keV higher T_{ion} and a factor of 3.2 yield increase relative to the average of the two unmagnetized implosions. This is significantly outside the 10% uncertainty in the T_{ion} measurement. The electron temperatures (uncertainty of $\sim$ 0.15 keV) show a similar increase, are typically slightly below the ion temperature and are derived by fitting the bremsstrahlung emission measured at three different x-ray energies ranging from 20 to 30 keV [44] assuming an isobaric radial temperature and density profile. The $B = 0$ experiment, N210717, had a Cu coil included in the target but no pulsed power; unmagnetized shot N210912 did not include a coil. Modeling shows that the coil produces no measurable change in the neutron trajectories. Magnetized shot N210301 used a capsule gas mix of 70% ^{4}He and 30% D, chosen to give a brighter core image from the higher Z of He. Sufficient core brightness allowed the subsequent shots to use pure D_2 gas to increase the secondary neutron yield. Figures 2 (b) - (d) show the equatorial view of the x-ray shape at maximum compression ("bang-time") for three of the experiments; shot N210717 had no shape data due to a section of Cu wire blocking the diagnostic view. The x-ray images are recorded at a sequence of times using a 50 ps gated detector sensitive from 4 - 8 keV [45, 46]. Fill-tube emission, visible in Figs. 2 (c) and (d) as a brighter region on the left of the images, is brighter than the surrounding hot-spot for the unmagnetized shot compared to the magnetized one. Future experiments will investigate the possible fill-tube mix mitigation from the B-field.

The laser pulse shape for magnetized shot N210301 was identical to N161204 (the earlier ignition design [38]), except with lower power (1 TW/beam) late in time [see Fig. 1 (b)] to reduce optics damage risk from Brillouin backscatter. The result was a large prolate shape. This was successfully corrected to nearly round on N210607 by reducing the cone fraction ($CF = E_{in}/E_{total}$ where E_{in} is the inner cone laser energy) from 0.27 to 0.23. Unmagnetized shot N210912 used the same laser pulse as N210607, except that two of NIFs 48 laser quads were dropped due to shot-time issues. The implosion shape was moderately oblate with $P_2/P_0 = -0.17$ where the equatorial shape is described analytically using Legendre polynomials P_0 and P_2. Post-shot hohlraum modeling of N210912 with the dropped quads re-instated gives a small hot-spot shape change of $\Delta P_2/P_0 = -0.03$. Previous measurements on 8 NIF unmagnetized D_2 gas-filled HDC capsule implosions at $\sim$ 1 MJ show that for hot-spot shape asymmetries with $|P_2/P_0| < 0.23$ the ion temperature varies by $\Delta T/T = \pm 0.06$ and the neutron yield by $\Delta Y_n/Y_n = \pm 0.14$ indicating the moderately oblate shape of N210912 produces only modest effects on T_{ion} and Y_n. D_2 gas-capsule implosions typically show 10 to 20% shot-to-shot variation in T_{ion} and Y_n demonstrating a robustness to laser delivery and target variability unlike the recent burning/igniting DT layered implosions which are on an ignition cliff. Capsule-only simulations with Gorgon (discussed below) corresponding to magnetized shot N210607 show that turning off the B-field with no change in the x-ray drive results in an oblate hot-spot shape with $P_2/P_0 = -0.17$, similar to the experiment. The imposed field could also change the x-ray drive asymmetry, for instance by altering cross-beam energy transfer (CBET) [47–49] either by changing plasma

conditions or the CBET coupling directly. Future experiments are needed to fully understand how the B-field influences hot-spot shape.

Pre and post-shot modeling uses the 2-D magneto-radiation-hydrodynamic code Lasnex [50, 51]. The code includes Nernst and Righi-Leduc B-field advection as well as resistive diffusion, magnetized thermal conduction and the Lorentz force. Simulations use a laser power and CF multiplier at peak laser power; this accounts for what is historically a somewhat lower x-ray drive in the experiment than in the simulations [52] and for the base level of cross-beam power transfer from outer to inner beams due to plasma flow. The multipliers are determined by matching the simulations to the measured capsule bang-time and equatorial P_2 shape. The simulated T_{ion} is plotted in Fig. 2 (a) and shows a generally good match to the three data points with shape measurements. The average *change* in the measured yield (3.2×) with magnetization is also approximately matched by the simulated yield change $\sim 2.5\times$; however, the absolute yield is significantly overestimated by the model. Current detailed hot-spot analysis is quantifying the effect of preheat and mix as possible yield degradation mechanisms. Analytical formulas [23] verified using the 2D Gorgon extended magneto-hydrodynamic code [23, 53–55] show that the temperature scales as $\sim \kappa_{eff}^{-2/7} = 1.37$ and yield amplification as $\sim \kappa_{eff}^{16/21} \exp[18.76(1-\kappa_{eff}^{2/21})/T_{B=0}^{1/3}] \sim 1.8$ where we assume fully magnetized with $\kappa_{eff} = 1/3$, full radiation transport and similar P_2 magnitudes as observed in experiments.

Increased ion temperature due to magnetic insulation is expected to be the same between gas-filled and DT ice layered implosions [23]. This is backed up in Lasnex simulations of the NIF ignition shot [1] where applying the NIF cryo design seed field of 40 T increases the ion temperature by 40% and the yield by a factor of ~ 2 [56]. The implosion has $CR \sim 22.8$ (initial capsule ID = 1050 μm) with peak mass-weighted hot-spot $T_{ion} \sim 14$ keV (unmagnetized is 10.5 keV), $\rho R \sim 0.45$ gm/cm^2 and volume-average $B \sim 24$ kT. The unmagnetized simulations are degraded with preheat to match the measured performance and the same degradation is applied to the magnetized simulations. A significant difference in the DT-layered implosions is the magnetization of the 3.5 MeV fusion alphas which further increases the yield. Additional benefits from magnetized mix suppression are expected [20] which could lead to larger T_{ion} and neutron yields. These initial experimental results on gas-capsules make a convincing case for testing magnetized cryo-layered implosions on NIF and open the door to new implosion designs specifically tailored for use with a B-field. Magnetized cryo layered implosions also require overcoming several significant technological challenges. These include successful *slow growth* of a spherical DT ice layer in the environment of a temperature controlled hohlraum current coil and maintaining a sufficiently unperturbed ice layer when the capsule and fuel are exposed to the *rapid* radiative heating from the ~ 500 K hohlraum wall temperature at the onset of the 40 T magnetization current. Additionally, the 2-layered solenoid coil design and cable transitions from the coax lines at the pulser to strip-lines and eventually the target coil wires must remain arc-free for the 5 s required to achieve peak current and ~ 40 T. Detailed simulations and lab tests show that we can overcome these challenges.

Lasnex simulations show an amplified and spatially varying hot-spot B-field with an average magnitude of 4.5 - 5 kT. Experimental evidence for the hot-spot B-field magnitude can be obtained using the ratio of secondary (14.1 MeV) to primary (2.45 MeV) neutrons. Secondary neutron analysis was successfully used to interpret the magnetized liner inertial fusion experiments [12, 14] but there were insufficient secondaries to be useful in the direct drive experiments [8]. A uniform 0-D Monte Carlo (MC) simulation for deuteron and triton transport through the fuel, including D-D and D-T fusion events, gives a deuteron fuel $\rho R = 60$ mg/cm^2 using the measured $Y_{DT}/Y_{DD} = 0.0125$ for the unmagnetized implosion N210912 [43]. This ρR value corresponds to compressing an initial capsule of inner radius 840 μm with 3.9 mg/cc of D_2 fill density to a final radius of 62 μm (0-D assumption), which is slightly larger than the measured x-ray hot-spot size of 55 μm. The X-ray and neutron hot-spot radii are not expected to be the same due to different temperature dependence. Magnetized implosion N210607 with $T_e = 4.3$ keV has $Y_{DT}/Y_{DD} = 0.012$; we estimate the same ρR as the unmagnetized case due to a similar P_0 in both x-ray measurements and Lasnex simulations. Using the MC simulation model a magnetic field of 4.7 ± 1.4 kT is consistent with the measured Y_{DT}/Y_{DD}, assuming a +/- 10% uncertainty in ρR and in the measured Y_{DT}/Y_{DD}.

In summary, magnetized gas-capsule implosions on NIF increase T_{ion} by 1.1 keV and the yield a factor of 3.2. Post-shot simulations approximately reproduce the ion temperature and yield increase for a $B = 26$ T applied field. The compressed B-field in the core is estimated from secondary neutron yield to be 4.7 ± 1.4 kT. Near-term experiments are planned on gas-filled capsules to improve understanding of magnetized implosions for a higher temperature hot-spot initially at 4 keV and to quantify the effect of magnetization on fill-tube and ablator-gas mix. We are also preparing to test the effect of magnetizing cryogenic D-T layered implosions on NIF.

This work was performed under the auspices of the U.S. Department of Energy by Lawrence Livermore National Laboratory under Contract DE-AC52-07NA27344 and by the LLNL-LDRD program under Project Number 20-SI-002.

TABLE I. Experimental and simulation results

NIF shot	N201228-001	N210301-001	N210607-002	N210620-001	N210717-001	N210912-001
Data						
E_{laser} (kJ)	924	926	883	867	875	840
Cone Fraction	0.27	0.27	0.23	0.23	0.23	0.22
Capsule fill (mg/cc)	none	30%D 70%^{4}He at 5.1	D at 3.99	none	D at 3.89	D at 3.99
B_{z0} (T)	0	26.1 ± 3.2	26.1 ± 3.2	0	0	0
T_{ionDD} (keV)		4.2 ± 0.14	3.8 ± 0.14		2.67 ± 0.14	2.72 ± 0.14
Y_{DD}		$(4.8 \pm 0.2)\times10^{11}$	$(2.0 \pm 0.1)\times10^{13}$		$(5.3 \pm 0.2)\times10^{12}$	$(6.7 \pm 0.3)\times10^{12}$
Y_{DT}/Y_{DD} ($\times10^{-2}$)		0.3 ± 0.04	1.2 ± 0.1		1.0 ± 0.1	1.3 ± 0.1
T_e (keV)		4.3 ± 0.2	3.4 ± 0.1		2.5 ± 0.1	2.5 ± 0.1
X-ray bangtime (ns)		7.48 ± 0.05	7.65 ± 0.05		7.75 ± 0.05	8.0 ± 0.05
P_0 (μm)		51 ± 3	54 ± 3			55 ± 3
P_2 (μm)		32 ± 3	3 ± 3			-10 ± 3
$CR = R_0/P_0$		16.55 ± 1	15.6 ± 0.9			15.3 ± 0.8
Lasnex simulation						
Y_{DD}		1.12×10^{12}	5.13×10^{13}		3.01×10^{13}	1.92×10^{13}
T_{ionDD} (keV)		3.66	3.71		2.98	2.74

[1] H. Abu-Shawareb, et al., "Lawson criterion for ignition exceeded in an inertial fusion experiment," Phys. Rev. Lett. 129, 075001, 2022.

[2] L. J. Perkins et al., The potential of imposed magnetic fields for enhancing ignition probability and fusion energy yield in indirect-drive inertial confinement fusion, Phys. Plasmas 24, 062708 (2017).

[3] A. Zylstra, O. Hurricane, et al., "Burning plasma achieved in inertial fusion," Nature 601, 542 (2022), https://doi.org/10.1038/s41586-021-04281-w.

[4] A. Kritcher, C. Young, H. Robey, et al., "Design of inertial fusion implosions reaching the burning plasma regime," Nature Physics (2022), 10.1038/s41567-021-01485-9, https://doi.org/10.1038/s41567-021-01485-9.

[5] J. G. Linhart et al., Amplification of magnetic fields and heating of plasma by a collapsing metallic shell, Nucl. Fusion Suppl. 2, 733 (1962); https://www.osti.gov/biblio/4726225.

[6] S. A. Slutz et al., Pulsed-power-driven cylindrical liner implosions of laser preheated fuel magnetized with an axial field, Phys. Plasmas 17, 056303 (2010).

[7] J. P. Knauer et al., Compressing magnetic fields with high-energy lasers, Phys. Plasmas 17, 056318 (2010).

[8] P. Y. Chang, G. Fiksel, M. Hohenberger, J. P. Knauer, R. Betti, F. J. Marshall, D. D. Meyerhofer, F. H. Sguin, and R. D. Petrasso, Fusion yield enhancement in magnetized laser-driven implosions, Phys. Rev. Lett. 107, 035006 (2011).

[9] M. Hohenberger, P.-Y. Chang, G. Fiksel, J. P. Knauer, R. Betti, F. J. Marshall, D. D. Meyerhofer, F. H. Seǵuin, and R. D. Petrasso, "Inertial confinement fusion implosions with imposed magnetic field compression using the OMEGA Laser," Phys. Plasmas **19**, 056306 (2012); https://doi.org/10.1063/1.3696032.

[10] L. J. Perkins, B. G. Logan, G. B. Zimmerman, and C. J. Werner, Phys. Plasmas 20, 072708 (2013).

[11] M. R. Gomez, S. A. Slutz, A. B. Sefkow, D. B. Sinars, K. D. Hahn, S. B. Hansen, et al., Experimental demonstration of fusion-relevant conditions in magnetized liner inertial fusion, Phys. Rev. Lett. 113, 155003 (2014).

[12] P. F. Schmit, P. F. Knapp, S. B. Hansen, M. R. Gomez, K. D. Hahn, D. B. Sinars, et al., Understanding fuel magnetization and mix using secondary nuclear reactions in magneto-inertial fusion, Phys. Rev. Lett. **113**, 155004 (2014).

[13] D. J. Strozzi, L. J. Perkins, M. M. Marinak, D. J. Larson, J. M. Koning, B. G. Logan, J. Plasma Phys. 81, 475810603 (2015).

[14] P. F. Knapp et al., Effects of magnetization on fusion product trapping and secondary neutron spectra, Phys. Plasmas **22**, 056312 (2015).

[15] D. H. Barnak, J. R. Davies, R. Betti, M. J. Bonino, E. M. Campbell, V. Yu. Glebov et al., Phys. Plasmas 24, 056310 (2017).

[16] J. R. Davies et al., Laser-driven magnetized liner inertial fusion, Phys. Plasmas 24, 062701 (2017).

[17] M. R. Gomez, S. A. Slutz, C. A. Jennings, D. J. Ampleford, M. R. Weis, C. E. Myers, et al., Performance scaling in magnetized liner inertial fusion experiments, Phys. Rev. Lett. 125, 155002 (2020).

[18] A. Bose, J. Peebles, C. A. Walsh, J. A. Frenje, N. V. Kabadi, P. J. Adrian, G. D. Sutcliffe, M. Gatu Johnson, C. A. Frank, J. R. Davies, *et al*, "Effect of Strongly Magnetized Electrons and Ions on Heat Flow and Symmetry of Inertial Fusion Implosions," Phys. Rev. Lett 128, 195002 (2022).

[19] C.A. Walsh, A.J. Crilly and J.P. Chittenden, Nucl. Fusion **60** 106006.

[20] C. A. Walsh, Magnetized Ablative Rayleigh-Taylor Instability in 3-D, Phys. Rev. E 105, 025206 (2022).

[21] J. D. Moody, "Boosting Inertial-Confinement-Fusion Yield with Magnetized Fuel," physics.aps.org, 2021, American Physical Society, May 5, 2021, Physics 14, 51, DOI: 10.1103/Physics.14.51.

[22] D. D.-M. Ho, L. J. Perkins, G. B. Zimmerman, G. Kagan, J. D. Salmonson, B. G. Loga, D. T. Blackfield, and M. A. Rhodes, 43rd European Physical Society (EPS) Conference on Plasma Physics (2016).

[23] C. A. Walsh, S. ONeill, J. P. Chittenden, A. J. Crilly, B. Appelbe, D. J. Strozzi, D. Ho, H. Sio, B. Pollock, L. Divol, E. Hartouni, M. Rosen, B. G. Logan, and J. D. Moody, Phys. Plasmas **29**., 042701 (2022); doi: 10.1063/5.0081915.

[24] S. I. Braginskii, in Reviews of Plasma Physics, edited by M. A. Leontovich (Consultants Bureau, New York, 1965), Vol. 1, P. 205.

[25] C. A Walsh and D. S. Clark, "Biermann battery magnetic fields in ICF capsules: Total magnetic flux generation," Phys. Plasmas **28**, 092705 (2021); doi: 10.1063/5.0059366.

[26] H.-S. Bosch and G.M. Hale, "Improved formulas for fusion cross-sections and thermal reactivities," 1992 Nucl. Fusion **32** 611 (1992).

[27] S. P. Regan, R. Epstein, B. A. Hammel, L. J. Suter, H. A. Scott, M. A. Barrios, et al, Phys. Rev. Lett. 111, 045001 (2013).

[28] T. Ma et al., Phys. Rev. Lett. 111, 085004 (2013).

[29] B. A. Hammel, *etal*, High Energy Density Physics 6, 171 (2010).

[30] D. S. Clark, *etal*, Phys. Plasmas 18, 082701 (2011), https://doi.org/10.1063/1.3609834.

[31] V. Smalyuk, *etal*, High Energy Density Physics 36, 100820 (2020).

[32] G. H. Miller, E. I. Moses, and C. R. Wuest, "The National Ignition Facility: Enabling fusion ignition for the 21st century," Nucl. Fusion 44, S228 (2004).

[33] A. Engwall et al., U.S. Patent Application No. 62/928968 (October 31, 2019) Lawrence Livermore National Security, LLC, High-resistivity metal alloy coatings fabricated with physical vapor deposition.

[34] L.B. Bayu Aji, A.M. Engwall, J.H. Bae, A.A. Baker, J.L. Beckham, S.J. Shin, X. Lepro Chavez, S.K. McCall, J.D. Moody, and S.O. Kucheyev, "Sputtered Au-Ta films with tunable electrical resistivity," J. Phys. D: Appl. Phys. **54**, 075303 (2021).

[35] A.M. Engwall, L.B. Bayu Aji, A.A. Baker, S.J. Shin, J.H. Bae, S.K. McCall, J.D. Moody, and S.O. Kucheyev, "Effect of substrate tilt on sputter-deposited $AuTa_4$ films," Appl. Surf. Sci. **547**, 149010 (2021), https://doi.org/10.1016/j.apsusc.2021.149010.

[36] J.H. Bae, L.B. Bayu Aji, S.J. Shin, A.M. Engwall, M.H. Nielsen, A.A. Baker, S.K. McCall, J.D. Moody, and S.O. Kucheyev, "Gold-tantalum alloy films deposited by high-density-plasma magnetron sputtering," J. Appl. Phys. **130**, 165301 (2021).

[37] J. D. Moody et al., Transient magnetic field diffusion considerations relevant to magnetically assisted indirect drive inertial confinement fusion, Phys. Plasmas 27, 112711 (2020).

[38] K. L. Baker, C. A. Thomas, D. T. Casey, S. Khan, B. K. Spears, R. Nora, et al., High-performance indirect-drive cryogenic implosions at high adiabat on the National Ignition Facility, Phys. Rev. Lett. **121**, 135001 (2018).

[39] G. E. Kemp , M. S. Rubery, C. D. Harris, M. J. May, K. Widmann, R. F. Heeter, S. B. Libby, M. B. Schneider, and B. E. Blue, "A genetic algorithm approach for reconstructing spectral content from filtered x-ray diode array spectrometers," Rev. Sci. Instrum. 91, 083507 (2020); https://doi.org/10.1063/5.0019059.

[40] L. Ballabio, J. K. Allne, and G. Gorini, Nuclear Fusion 38, 1723 (1998).

[41] V. Y. Glebov, *et al*, Rev. Sci. Instrum. 81, 10D325 (2010), https://doi.org/10.1063/1.3492351.

[42] R. Hatarik, *et al* Journal of Applied Physics 118 (2015), 10.1063/1.4935455.

[43] H. Sio, J. D. Moody, D. D. Ho, B. B. Pollock, C. A. Walsh, B. Lahmann, D. J. Strozzi, G. E. Kemp, W. W. Hsing, A. Crilly, J. P. Chittenden, and B. Appelbe, Rev. Sci. Instrum. 92, 043543 (2021); https://doi.org/10.1063/5.0043381.

[44] B. Bachmann *et al*, Physical Review E 101, 033205.

[45] S. Glenn, J. Koch, D. K. Bradley, N. Izumi, P. Bell, J. Holder, G. Stone, R. Prasad, A. MacKinnon, P. Springer, O. L. Landen, and G. Kyrala, A hardened gated x-ray imaging diagnostic for inertial confinement fusion experiments at the National Ignition Facility, Rev. Sci. Instrum. 81, 10E539-10E532 (2010).

[46] G. A. Kyrala, S. Dixit, S. Glenzer, D. Kalantar, D. Bradley, N. Izumi, N. Meezan, O. L. Landen, D. Callahan, S. V. Weber, J. P. Holder, S. Glenn, M. J. Edwards, P. Bell, J. Kimbrough, J. Koch, R. Prasad, L. Suter, J. L. Kline, and J. Kilkenny, Measuring symmetry of implosions in cryogenic Hohlraums at the NIF using gated x-ray detectors, Rev. Sci. Instrum. 81, 10E31610E323 (2010).

[47] Kruer, W. L., Wilks, S. C., Afeyan, B. B. and Kirkwood, Robert K. "Energy transfer between crossing laser beams," Phys. Plasmas 3, 382385 (1996).

[48] Michel, P. et al. "Tuning the implosion symmetry of ICF targets via controlled crossed-beam energy transfer" Phys. Rev. Lett. 102, 025004 (2009).

[49] J. D. Moody, et al., Multistep redirection by cross-beam power transfer of ultrahigh-power lasers in a plasma, Nature Phys. 8, 344 (2012).

[50] G. Zimmerman and W. L. Kruer, "Numerical Simulation of Laser-Initiated Fusion," Comments Plasma Phys. Controlled Fusion 2, 85 (1975).

[51] J. Nuckolls, L. Wood, A. Thiessen, and G. B. Zimmerman, Nature, 239, 5368, pp. 139142 (1972).

[52] O. S. Jones, L. J. Suter, H. A. Scott, M. A. Barrios, W. A. Farmer, S. B. Hansen, D. A. Liedahl, C. W. Mauche, A. S. Moore, M. D. Rosen, J. D. Salmonson, D. J. Strozzi, C. A. Thomas, and D. P. Turnbull, Phys. Plasmas 24, 056312 (2017); https://doi.org/10.1063/1.4982693.

[53] A. Ciardi, S. V. Lebedev, A. Frank, E. G. Blackman, J. P. Chittenden, C. J. Jennings, D. J. Ampleford, S. N. Bland, S. C. Bott, J. Rapley, G. N. Hall, F. A. Suzuki-Vidal, A. Marocchino, T. Lery, and C. Stehle, The evolution of magnetic tower jets in the laboratory, Phys. Plasmas 14, 056501 (2007).

[54] J. P. Chittenden, N. P. Niasse, S. N. Bland, G. A. Hall, S. V. Lebedev, and C. A. Jennings, Recent advances in magneto-hydrodynamic modeling of wire array Z-pinches, in IEEE International Conference on Plasma Science (IEEE, 2009).

[55] C. A. Walsh, J. P. Chittenden, K. McGlinchey, N. P. L. Niasse, and B. D. Appelbe, Self-generated magnetic fields in the stagnation phase of indirect- drive implosions on the National Ignition Facility, Phys. Rev. Lett. 118, 155001 (2017).

[56] D. D. Ho, G. B. Zimmerman, A. L. Velikovich, R. M. Kulsrud, J. D. Moody, J. Harte, and A. L. Kritcher, Magnetized ICF: role of e-thermal conductivity on imploding shock and high-yield capsule designs, 63rd Annual Meeting of the APS Division of Plasma Physics, UO04.00010, 2021.